13.3

RESOLVING A FOREST-STRIP INDUCED INCREASED UPLIFT REGION USING THE SHAVED-GRID CELL METHOD WITH LARGE EDDY SIMULATIONS

Vasilia Velissariou*[1], Gil Bohrer[1]

[1]Civil & Environmental Engineering & Geodetic Science,The Ohio State University,Columbus, OH

ABSTRACT

The RAMS-based Forest Large Eddy Simulation (RAFLES) resolves flows inside and above forested canopies. RAFLES is spatially explicit, and uses the finite volume method to solve a descretized set of Navier-Stokes equations. It accounts for vegetation drag effects on the flow and on the flux exchange between the canopy and the canopy air, proportional to the local leaf density. For a better representation of the vegetation structure in the numerical grid within the canopy sub-domain, the model uses a modified version of the shaved-grid coordinate system. The hard volume of vegetation elements within each numerical grid cell is represented via a sub-grid-scale process that shrinks the open apertures between grid cells and reduces the open cell volume. The model uses lidar scans of forests combined with empirical biological structural data to derive explicit or simplified, 3D heterogeneous simulation domains that include leaf density and stem.

We used RAFLES to simulate the effects of forest strips of varying foliage and stem densities on flow over these barriers under neutrally buoyant conditions. We explicitly tested the effects of the numerical representation of hard volumes, independent of the effects of the leaf drag. The results show that flow through semi-porous forest barriers leads to increased uplift both at the upwind face and downwind of the barrier. Introduction of volume restriction in the flow dynamics shifted the location of the downwind uplift zone and anchored it to the downwind edge of the barrier.

*Corresponding author address: Vasilia Velissariou, The Ohio State University, Dept. of Civil & Environmental Engineering & Geodetic Science, Columbus, OH 43210; e-mail: velissariou.3@osu.edu.

1. INTRODUCTION

The flow inside and around tall forests is a subject that receives growing attention in various research areas and finds many applications such as the study of the emission and dispersion of particles and gases through and over a windbreak (Bergen,1975, Prueger et al, 2008), study of tree stand stability and resistance to breakage (Gardiner et al., 1997, Dupont and Brunet, 2006, 2008a) and study of the effectiveness of trees as wind breakers (Santiago, et al., 2007). Studies of the meteorological boundary layer structure above forest edges (Liu et al.,1995, Patton et al., 1998, Belcher et al., 2003, Yang et al., 2006, Cassiani et al., 2008, Dupont and Brunet, 2008b), have recognized the resemblance of a forest edge to either a forward or a backward facing step. Depending on the application, these studies have focused on the analysis of the approaching flow field or the exit flow field.

The problem has been studied experimentally and with models, via analyses of field data, data from air tunnel experiments over artificial canopies or from various model simulations. The tool for our analysis is the RAMS-based Forest Large Eddy Simulation (RAFLES). An important feature of the model is the ability to represent both the effects of drag, primarily from leaf surfaces, and of volume restriction to airflow in the canopy sub-domain, mostly from stems and branches.

The focus of the present study is to examine the disturbances on the flow caused by the transition from a clearing to a forest and the disturbances caused by the transition from the forest to a clearing. We also test the effects of including the volume restriction in the dynamic core of the model, which is a new approach compared to classic approaches that assigned only a drag as a canopy representation.

2. THE MODEL

RAFLES was developed and evaluated by Bohrer et al., (2009). It explicitly resolves flow inside and above realistic three-dimensional (3-D) heterogeneous canopies. RAFLES is based on the RAMS model, a regional atmospheric model that can operate at the resolution needed for Large Eddy Simulations (LES) (Avissar et al. 1998; Avissar and Schmidt 1998). RAFLES solves the 3-D Navier–Stokes equations on a rectangular, vertically stretched grid mesh, using a quasi-hydrostatic approach and the Boussinesq approximation. RAFLES includes a multi-layer, 3-D heterogeneous canopy, allowing for the effects of leaves and stems on flow momentum through drag and the volume and aperture restriction pause by the physical barriers created by the stems and branches acting. The canopy in RAFLES also acts as a source for latent and sensible heat fluxes the drag and fluxes.

In LES model variables are decomposed into two components, a resolved (mean) grid-averaged component, and a perturbation from that mean known as the sub-grid scale (SGS) perturbation. Applying such a partitioning between the resolved and the SGS components of the Navier–Stokes equations leads to the following prognostic equation for the resolved scale velocity written here in flux form and using Einstein notation:

$$\frac{\partial \bar{u}_i}{\partial t} + \frac{1}{\rho_o}\left[-\frac{\bar{u}_\iota \partial\left(\rho_o \bar{u}_j\right)}{\partial x_j} + \frac{\partial\left(\rho_o \bar{u}_i \bar{u}_j\right)}{\partial x_j} + \frac{\partial\left(\rho_o \overline{u_i' u_j'}\right)}{\partial x_j}\right] = \delta_{i3} g \frac{\overline{\theta_{vp}}}{\theta_{v0}} - \theta_0\left(\frac{\partial \bar{\pi}_p}{\partial x_i}\right) + F(\bar{u}_i) + D_i(\bar{V}) \qquad (1)$$

where, $\bar{u}_i$ is the resolved wind velocity, ρ_o is the air density, t is the time, g is the gravitational acceleration, δ is the Kronecker delta, θ_{vp} is the potential virtual temperature, θ_{vo} is a reference potential virtual temperature (used at model initialization, horizontally homogeneous and constant in time), π_p is the pressure expressed in terms of the Exner function (Klemp and Wilhelmson, 1978) and see exact form used in RAFLES in Bohrer et al. (2009), $D_i(\bar{V})$ represents the components of the canopy drag force per unit mass that are function of the resolved-scale velocity and $F(\bar{u}_i)$ represents the sum per unit mass of horizontal wind forcing through the domain, which is comprised of Rayleigh friction and of a Newtonian nudging described in Bohrer et al., (2009).

For comparable horizontal and vertical grid sizes the turbulence momentum tendencies are:

$$\left.\frac{\partial \mathrm{u_i}}{\partial \mathrm{t}}\right|_{\mathrm{turb}} = -\frac{1}{\rho_o}\frac{\partial\left(\rho_o \overline{u_i' u_j'}\right)}{\partial x_j} \qquad (2)$$

summation over j; (i,j) = (1,2,3).

Using the full expansion for $\overline{u_i' u_j'}$ described in Deardorff (1980), the sub-grid scale (SGS) stresses are evaluated by the following equation:

$$\overline{u_i' u_j'} = -K_m\left(\frac{\partial \bar{u}_i}{\partial x_j} + \frac{\partial \bar{u}_j}{\partial x_i}\right) + \frac{2}{3}\delta_{ij}\bar{e} + \overline{u_i' u_j'}|_{surf} \qquad (3)$$

where, K_m is the momentum eddy diffusivity defined as: $K_m = 0.1 l_e \bar{e}^{1/2}$, l_e is an empirical length scale for mesh size and dissipation defined as in Bohrer et al., (2009) and $\bar{e}$ is the turbulent kinetic energy defined as $\bar{e} = \overline{u_i' u_i'}/2$. The last term on the right hand side of equation (3) represents the additional vertical fluxes imposed at the surface. This term is zero everywhere except at the top and the bottom boundaries and it is included here for completeness. For the bottom boundary, the term is evaluated numerically at the first two grid points above the surface.

Equations (2) and (3) are solved in a two-step process using a tri-diagonal solver for the "vertical" terms (implicit part of the solution), subsequently adding the "horizontal" terms (explicit part of the solution) to calculate the final solution for the momentum rate of change at the current computational time-step. This two-step solution has replaced the one-step explicit solution previously used in RAFLES.

Formulation of the SGS turbulent kinetic energy (TKE) $\bar{e}$ is based on the equation given in Deardorff, (1980):

$$\frac{\partial \bar{e}}{\partial t} + \frac{\partial\left(\rho_o \bar{u}_j\, \bar{e}\right)}{\rho_o \partial x_j} + \frac{\bar{e}}{\rho_o}\frac{\partial\left(\rho_o \overline{u_j}\right)}{\partial x_j} = \frac{g}{\theta_v}\overline{w'\theta_v'} - \overline{u_i' u_j'}\frac{\partial u_i}{\partial x_j} - \frac{\partial}{\partial x_i}\left[\overline{u_\iota'\left(e + \frac{p'}{\bar{\rho}}\right)}\right] - \frac{8}{3} C_{dl} A_l |\bar{V}| \bar{e} - \varepsilon \qquad (4)$$

The first term on the right hand side is a buoyancy production or consumption term, which is positive when the heat flux is positive and negative otherwise. The second term on the right hand side is the shear production or consumption term. The fourth term represents the contribution of the canopy to the drag on SGS motion (Shaw and Patton, 2003) and the fifth term accounts for

the viscous dissipation (see Bohrer et al., (2009) for the dissipation parameterization).

RAFLES uses a shaved grid-cell finite volume discretization (Adcroft et al. 1997; Walko and Avissar 2008). Applying the Gauss divergence theorem for a vector field $\vec{F}$, the control volume integrals of the gradient of a vector quantity can be transformed into surface integrals as follows:

$$\int_{\Psi} \nabla \cdot \vec{F}\, d\Psi = \int_{\sigma} \vec{F} \cdot d\vec{\sigma} = \int_{\sigma} \vec{F} \cdot \vec{n} d\sigma = \sum_{i=1}^{3} \frac{\dot{\Delta}(\sigma_i F_i)}{\Psi} \quad (5)$$

where, Ψ is the volume of the computational cell (the control volume), $\vec{n} = (n_x, n_y, n_z)$ are the unit normal vectors in the x, y, z directions and σ_x, σ_y, σ_z are the aperture areas normal to the x, y and z directions respectively. The aperture area σ represents the common area between two adjacent cells though which flow passes.

RAFLES uses a split-time leapfrog discretization scheme (Haltiner and Williams 1980) that allows different terms of the equation to be integrated at different time-step intervals (indicated in equation 6 by the superscript (t)). The pressure gradient term is integrated over a small time-step interval $\Delta t_s = \Delta t / N_{ts}$, where $N_{ts} \geq 1$ is the number of small time-steps t_s within each longer time-step t. An intermediate time-step t_m is applied to the advection and the turbulent tendency terms. The discretized momentum equation in space and time is given below and is solved using the Arakawa and Lamb, 1977, type C staggered grid scheme:

$$\begin{aligned} &\frac{\overline{u_i}^{(t+1)} - \overline{u_i}^{(t-1)}}{2\Delta t} \\ &+ \frac{M}{N_{ts}} \sum_{m=1}^{N_{ts}/M} \left[\frac{\dot{\Delta}_j}{\rho_o \Psi} \left(\left(\rho_o \sigma_j \overline{u_i}\, \overline{u_j}\right) - \overline{u_i}\left(\rho_o \sigma_j \overline{u_j}\right) \right.\right. \\ &\left.\left. - \rho_o \sigma_j K_m + \rho_o \sigma_j \frac{2}{3} \delta_{ij} \bar{e} \right)^{t-1+m\Delta t_m} \right] \\ &= F(\overline{u_i})^{(t)} + D_i(\overline{V})^{(t)} + \delta_{i3} g \frac{\overline{\theta_{vp}}^{(t)}}{\theta_{v0}} \\ &- \frac{\theta_0}{N_{ts}} \sum_{n=1}^{N_{ts}} \left[\left(\frac{\Delta \overline{\pi}_p}{\Delta x_i} \right)^{(t-1+n+\Delta t_s)} - \frac{\Delta \overline{\pi}_g}{\Delta x_i} \right] \end{aligned} \quad (6)$$

3. CANOPY STRUCTURE

In forest canopies, the flow field is affected by the drag due to both the tree leaves and the tree stems, by the exchange of heat and moisture between the canopy and the atmosphere and by space restrictions due to the tree stems. RAFLES' formulation of the heat and moisture interactions between the canopy and atmosphere is based on prescribed static rates, based on eddy-flux observations and redistributed in space as a function of leaf area index and light attenuation through the canopy. It is described in Bohrer, (2009). In this study we used neutrally buoyant conditions and therefore we did not prescribed heat or water vapor fluxes from the canopy.

For the formulation of the drag exerted by the canopy on the airflow, RAFLES uses canopy information about the 3-D leaf area density (LAD) distribution, the stem radius and the canopy top height. The drag force per unit air mass that the leafy portion of the canopy (D_l) exerts on the flow is formulated as described in Shaw and Schumann,(1992) and Shaw and Patton (2003) and was incorporated into RAFLES (Bohrer et al 2009) using:

$$D_{li} = -\left(C_{dl} + \frac{1.328}{(R_l)^{1/2}} \right) \left(\frac{A_l \Delta x_1 \Delta x_2}{\Psi} \right) |\bar{V}| \overline{u_i} \quad (7)$$

The drag force per unit air mass that the woody portion of the canopy (D_l) exerts on the flow is expressed as:

$$D_{wi} = \begin{cases} -C_{dl} \left(\dfrac{2\left(\Delta x_i \Delta x_3 - \sigma_j\right)}{\Psi} \right) |\bar{V}| \overline{u_i}\,, \\ \quad i = (1,2);\ j = (1,2);\ \ i \neq j, \\ -C_{dl} \left(\dfrac{2\sum\left(x_i \Delta x_j - \sigma_j\right)}{\Psi} \right) |\bar{V}| \overline{u_i}\,, \\ \quad i = 3;\ \ j = (1,2) \end{cases} \quad (8)$$

where, $|\bar{V}|$ is the wind speed magnitude, R_l is the Reynolds number, C_{dl} is an empirically derived vegetation skin drag coefficient and A_l is the leaf area per ground area of the canopy at each grid point.

The finite volume discretization method used for the momentum equation (1) introduces two additional variables in the discretized momentum equation (6), the cell volume and the aperture that need to be defined. The volume of each computation cell is reduced by an amount equal to the tree stem volume within the cell. Similarly, the surfaces areas on the cell faces are reduced by an amount equal to the projected tree stem area in the direction of each cell face.

Figure 1 illustrates the use of the shaved grid method in topographic representations (as in

Walko and Avissar 2008). Cell volume portions below ground are shown in brown, cell volumes completely above ground are shown in blue and cell volume portions above the ground in partially submerged grid cells are shaded.. Control volumes are labeled with Ψ and the corresponding control surfaces with σ. The control volumes are calculated as: Ψ = ΔxΔyΔz. For example, Ψ_{22} represents the control volume of an unobstructed cell. Ψ_{11}, Ψ_{21}, Ψ_{12} are reduced by an amount equal to the volume portion represented in brown in the corresponding grid cell such that: $\Psi_{11} < \Psi_{21} < \Psi_{12} < \Psi_{22}$ = unobstructed control volume. The apertures at the grid surface interfaces are also reduced such that: $0 = \sigma_{x01} < \sigma_{x11} < \sigma_{x21} < \sigma_{x02} < \sigma_{x12} = \sigma_{x22} = \Delta y\, \Delta z$ in the x direction and $0 = \sigma_{z10} = \sigma_{z20} < \sigma_{z11} < \sigma_{z21} = \sigma_{z12} = \sigma_{z22} = \Delta y\, \Delta x$ in the z direction. Flow through the control surfaces σ_{x01}, σ_{z10}, σ_{z20}, is totally restricted, through the control surfaces σ_{x12}, σ_{x22}, σ_{z21}, σ_{z12}, σ_{z22} is totally unrestricted and for the rest is partially restricted.

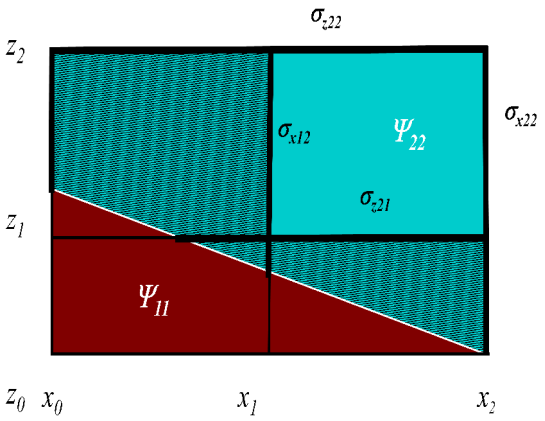

Figure 1: *The shaved cell method: topographic representation.*

In RAFLES, σ and Ψ are reduced wherever tree stems partially or completely obstruct a grid-cell face (Figure 2), leading to a proportional reduction in any flux across that face:

$$\sigma_i = \Delta x_j \Delta x_3 - 2 \int_{x_3 - 0.5\Delta x_3}^{x_3 + 0.5\Delta x_3} r_{x_3} \qquad (9)$$

$$and \;\; i = (1,2); i \neq j$$

$$\sigma_i = \Delta x_1 \Delta x_2 - max\left|\pi r_{x_3}^2\right|_{x_3 - 0.5\Delta x_3}^{x_3 + 0.5\Delta x_3} \qquad (10)$$

$$and \;\; i = 3$$

$$\Psi = \Delta x_1 \Delta x_2 \Delta x_3 - \pi \oint r_{x_3}^2 \qquad (11)$$

where, r_{x_3} is the vertical profile of stem radius in the cell. The obstacle-induced face reduction is considered uniform over the face, as if regulated by a Venetian blind. Similarly, volume reduction of a cell that contains a stem is considered uniform. The volume reduction leads to compression of the flow.

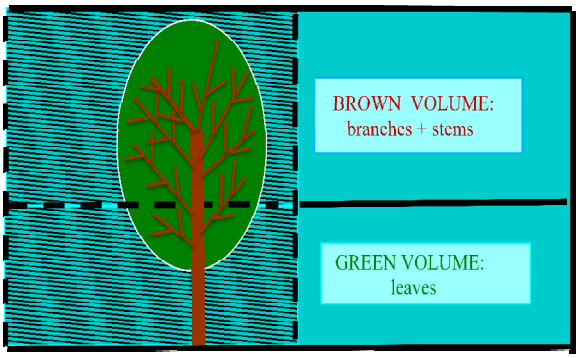

Figure 2: *The shaved cell method: canopy representation.*

4. BOUNDARY, INITIAL CONDITIONS AND THE EXPERIMENT SET UP

Periodic boundary conditions are applied at the lateral sides. A zero-flux condition and a free-slip condition for the horizontal velocity are applied at the top boundary. The vertical velocity at the top is zero. Rayleigh friction is applied to the upper five grid levels to reduce reflection. Free slip conditions for the horizontal velocity and zero vertical velocity are assumed at the bottom boundary. Surface momentum fluxes due to the soil friction are imposed at the bottom boundary for the three velocity components.

The model was initialized using horizontally homogeneous profiles of air pressure, potential temperature, humidity, air density and the horizontal components of wind. Initial profiles are based on similarity theory up to the neutrally mixed boundary layer. (in this case we assumed 200m) and Newtonian nudging of the wind above this layer (>200m) at 1m/s. The initial vertical component of wind velocity is set to zero and the initial SGS TKE is set equal to the minimum value of 0.0005 m^2/s^2.

Case no	Drag generating area density (m^2 drag area / m^3 air)	Simulation type	Stem diameter (m)	Aperture $\sigma_x/\Delta y\Delta z$	Volume Blockage %
1	0.02π	Drag only	1	1	0
2	0.04π	Drag only	2	1	0
3	0.06π	Drag only	3	1	0
4	0.08π	Drag only	4	1	0
5	0.02π	Control	1	4/5	20
6	0.04π	Control	2	3/5	40
7	0.06π	Control	3	2/5	60
8	0.08π	Control	4	1/5	80
9	0	Restriction only	1	4/5	20
10	0	Restriction only	4	1/5	80

Table 1*: Ten cases were simulated. The simulation time in all cases was set to 12 hours, which allowed the simulation to reach a quasi-stationary stage.*

The model domain for the present experiment was set to 0.5x0.5x1.4km^3 that resulted in 100x100x95 grid points. Horizontal grid resolution is 5x5m^2. Vertical grid resolution is 3m at the region between the ground and 100m. Above this height a 20% stretching is applied for each consecutive vertical layer up to a maximal grid spacing of 30m.

The barrier, representing a rather dense canopy, is represented by a block of about 27m in height, 125m in width and 125m in length. Tree stems are assumed to be equally spaced within the canopy block with one assumed cylindrical tree stem per vertical column located at the center of the column.

This set up results in homogeneous volume and aperture reductions for all the grid cells within the canopy sub-domain and symmetry between the horizontal faces, i.e., $\sigma_x = \sigma_y$. We ran ten simulation cases the characteristics of which are listed in Table 1. Simulations were run for 12 hours to achieve a quasi-stationary state and only data from the last 30 minutes were used in the analysis.

5. RESULTS AND DISCUSSION

Our discussion focuses on two extreme simulated canopy cases, the **sparse** (20% restriction by volume π m^2 drag generating area per m height) and the **dense** (80% restriction by volume π m^2 drag generating area per m height). For each canopy, we tested the effects of the drag and the volume restriction on the flow field by comparing **drag-only** simulations, where we prescribed no volume or aperture restriction to the flow, **restriction-only** simulations, where we prescribed no drag, and **control** simulations, where both drag and volume plus aperture restriction were included in the numerical core.

A. Effects on horizontal wind speed

Figure 3 shows the 2-D maps of the wind speed distribution on a plane intersecting the canopy block at a height 4.5m above the ground. The plots in Figure 3 shows strong evidence of a re-circulation zone (suggested by Detto et al. 2008) shortly downwind the canopy block in the drag only and drag and volume restriction cases for a sparse or a dense canopy.

Figure 4 shows typical vertical wind profiles obtained in each of the simulations, at selected locations across the domain, upwind, inside and downwind of the canopy. The profiles for the drag-only cases and control cases with either sparse or dense canopy (Figures 4a-b, 4d-e) as predicted (Yang et al., 2006), show a distinct point of inflection at a height equal to 0.75H, the effective displacement height of the canopy. Figures 4c and 4f show the effect of the volume restriction. The classical shear profile does not develop because in our model the canopy effect on momentum is enforced through drag with a free slip condition for horizontal velocity components is imposed at the bottom boundary. Since no drag is prescribed in these cases, the vertical profile of the flow is almost flat. Just upwind of the the beginning of the canopy the flow decelerates due to a pressure front formed by the compression of the flow into the canopy domain, where the volume is restricted. The dense canopy also shows acceleration of a sub-canopy jet inside the canopy sub-domain.

B. Effects on vertical wind velocity

Figure 5 shows contours of the laterally averaged vertical velocity (w), and the relative velocity u' defined at each point in the simulation domain as:

$$u' = \langle \bar{u} \rangle - \{\langle \bar{u} \rangle\} \quad (12)$$

where $\langle \bar{u} \rangle$ is the time averaged, laterally averaged wind speed at each grid point and $\{\langle \bar{u} \rangle\}$ is the ensemble average of $\langle \bar{u} \rangle$ in space, along each vertical layer of the simulation domain at a fixed height.

In all cases, a standing wave leading to uplift is formed at the front of the canopy. In the control cases (with volume restriction) there is also a corresponding narrow downwind re-circulation zone inside the canopy at the upwind edge of the canopy. An additional uplift area is formed at the downwind edge of the canopy, followed by a re-circulating downdraft zone. This effect is more pronounced in the sparse cases (compared with their equivalent dense cases) and it is very small in the control cases.

In the drag-only cases, an increased uplift region exists at a distance of roughly 2.5H (H is the length scale corresponding to the height of the canopy) downwind of the canopy start. In the control cases, this enhanced uplift zone is missing. However, a very strong coherent structure is formed above the canopy, at a height between 2-10H. A similar structure exists in the drag only simulations, but is is weaker and less organized.

6. CONCLUSIONS

Our simulations show that representation of the effects of the volume and aperture closure due to vegetated canopy and other semi-porous obstacles to flow is important. When the volume and aperture closure where represented, the location of coherent motion that is generated by the interaction of the flow with the obstacle became more fixed and that increased the strength of those coherent structures. This led to differences in the resolved strengths and locations of increased updraft zones between simulations, which included volume restriction, and those that included only drag. While improvements are still needed in the representation of drag in the canopy and its effects on resolved momentum and sub-grid scale turbulence in large eddy simulations, the representation of volume restriction due to the presence of the stems and branches is one improvement to LES dynamics that should be considered.

7. ACKNOWLEDGEMENTS

The work was funded by by The USDA Forest Service Northern Research Station Laboratory in Lansing MI (research joint venture agreement #: FS-NRS-06-Fire-10-01), USFS Northern Research Station in Delaware OH (agreement #: 09-CR-11242302-033), the U.S. Department of Energy's Office of Science (BER) through the Midwestern Regional Center of the National Institute for Climatic Change Research at Michigan Technological University award # DE-FC02-06ER64158, the US Department of Agriculture National Institute for Food and Agriculture, Air Quality grant #2010-65112-20564 and the National Science Foundation through grants # DEB-0911461 and DEB-0918869.

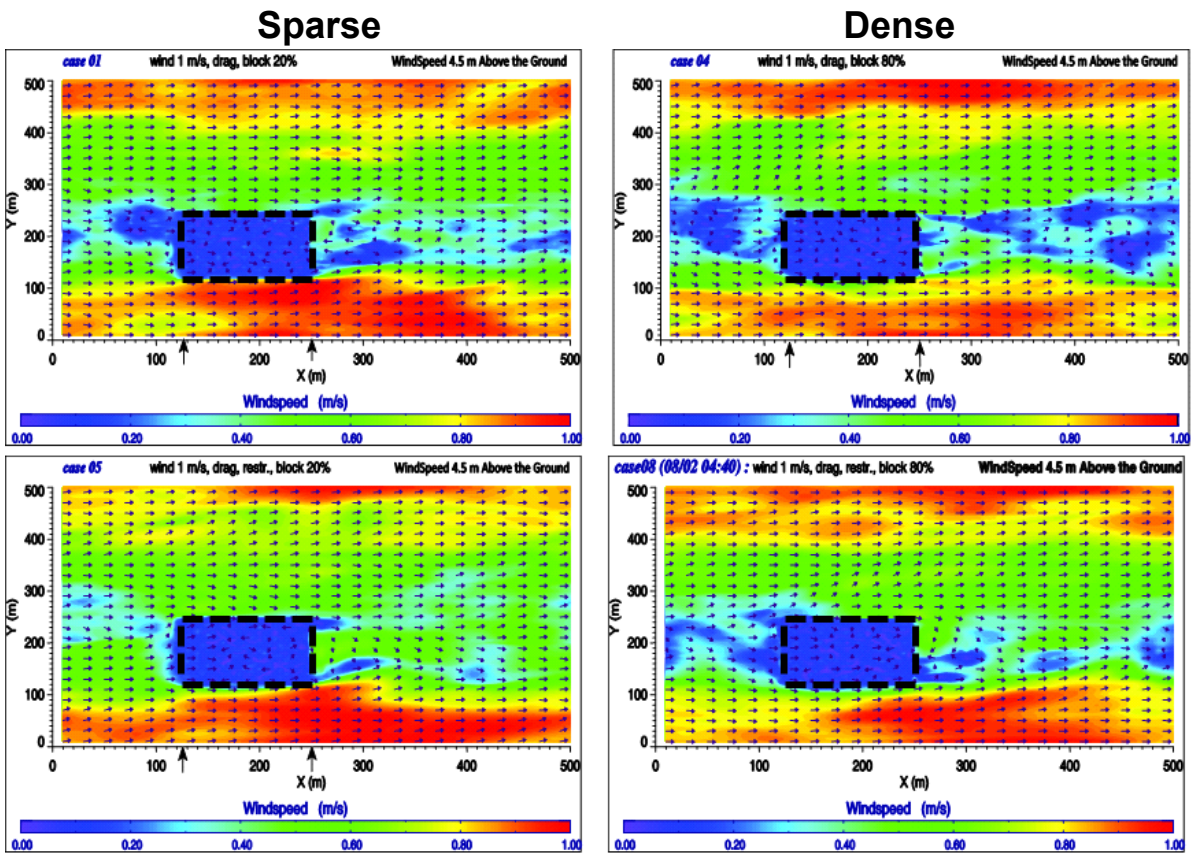

Figure 3: *Wind speed at 4.5 m above ground. Color represents the wind speed., arrows represent the horizontal wind velocity (with direction). Wind forcing was 1 m/s at 200 m above ground, at the X direction (right). The canopy is indicated by a dashed rectangle. Note that the X and Y direction in the simulation defined a square domain and a square canopy. The rectangular appearance is due to different scaling of the horizontal axes in the figure. The panels show the sparse (left column) and dense (right column) cases, with drag only (top panels) and control, with drag and volume restriction (bottom panels).*

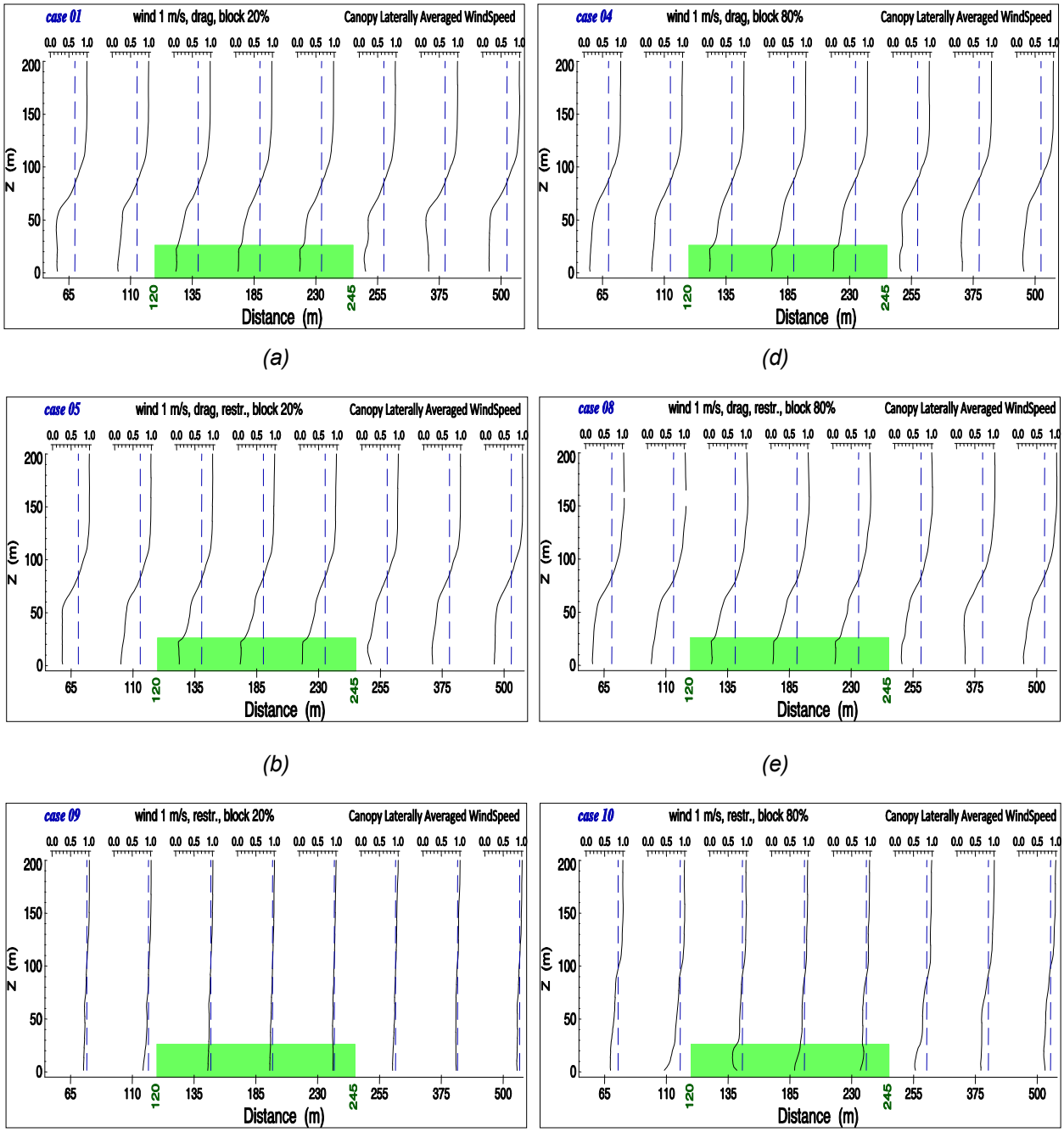

Figure 4: *Time averaged vertical wind speed profiles at selected locations in the sparse canopy cases (a) drag only, (b) control (c) restriction only and in the dense cases. (d) drag only, (e) control (f) restriction only The canopy domain is highlighted in green. Each profile represents an average of 30 minutes and an average across a horizontal section at the Y direction (into the image) over the central half of the canopy domain.*

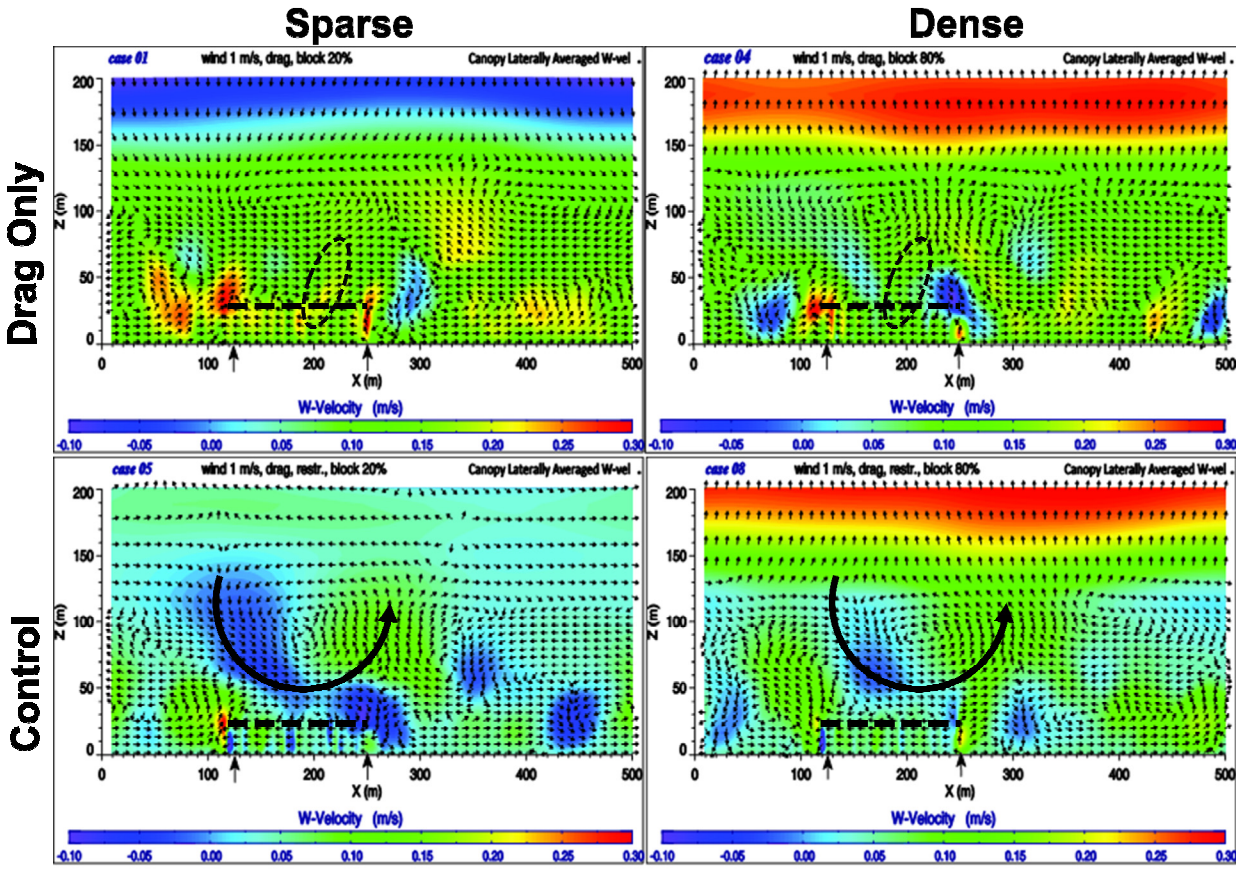

Figure 5: *u' and w illustrated across a vertical cross section through the simulation domain. The colors illustrate w. The arrows illustrate a vector whose horizontal component is u' and vertical component is w'. Canopy start (upwind) and end (downwind) are marked by arrows on the x-axis, and the canopy top (H) is marked by a thick dashed line. Sparse cases are illustrated on the left panels, dense on the right. Drag only simulations on the upper panels, control simulations on the bottom panels. Dashed ellipses in the drag only simulations illustrate the increased uplift zone at 2.5H downwind. A thick curved black arrow highlights the coherent structure above the canopy in the control simulations.*

REFERENCES

Adcroft A., Hill C., Marshall J., 1997: Representation of topography by shaved cells in a height coordinate ocean model. *Monthly Weather Review*, 125, 2293–2315.

Arakawa A., Lamb V.R., 1977: Computational design of the basic dynamical processes of the UCLA general circulation model. In: Chang J (ed): *Methods in computational physics: advances in research and applications*. Academic Press, London, pp 174–265.

Avissar R., Schmidt T., 1998: An evaluation of the scale at which ground-surface heat flux patchiness affects the convective boundary layer using large-eddy simulations. *Journal of Atmospheric Science*, 55:2666–2689.

Avissar, R., Eloranta E.W., Gurer K., and Tripoli G.J., 1998: An evaluation of the large-eddy simulation option of the regional atmospheric modeling system in simulating a convective boundary layer: a FIFE case study. *Journal of Atmospheric Science*, 55:1109–1130.

Belcher S.E., Jerram N, Hunt JCR, 2003: Adjustment of a turbulent boundary layer to a canopy of roughness elements. *Journal of Fluid Mechanics*, 488:369–398.

Bergen J.D., 1975: Air movement in a forest clearing as indicated by smoke drift. *Agricultural Meteorology*, 15:165-179.

Bohrer G., Katul G.G., Walko R.L., Avissar R., 2009: Exploring the Effects of Microscale Structural Heterogeneity of Forest Canopies Using Large-Eddy Simulations. *Boundary-Layer Meteorology*, 132:351–382, DOI 10.1007/s10546-009-9404-4.

Cassiani M., Katul G.G., Albertson J.D., 2008: The effects of canopy leaf area index on airflow across forest edges: large eddy simulation and analytical results. *Boundary-Layer Meteorology*, 126:433–460.

Deardorff J.W., 1980: Stratocumulus-capped mixed layers derived from a 3-dimensional model. *Boundary-Layer Meteorology*, 18:495–527.

Detto M., Katul G.G., Siqueira M., Juang J-H, Stoy P. C, 2008: The structure of turbulence near a tall forest edge: the backward facing step flow analogy revisited. *Ecological Applications*, 18: 1420–1435.

Dupont S. and Brunet Y., 2006: Simulation of turbulent flow in an urban forested park damaged by a windstorm. *Boundary-Layer Meteorology*, 120: 133-161.

Dupont S. and Brunet Y., 2008a: Impact of forest edge shape on tree stability: a large-eddy simulation study. *Forestry*, 81: 299-315.

Dupont S. and Brunet Y., 2008b: Edge flow and canopy structure: a large-eddy simulation study. *Boundary-Layer Meteorology*, 126:51–71 119: 377–412.

Gardiner B.A., Stacey G.R., Belcher R.E., and Wood C.J., 1997: Field and wind tunnel assessments of the implications of re-spacing and thinning for tree stability. *Forestry*, Vol. 70, No. 3, 233-252.

Haltiner, G.J. and R.T. Williams, 1979: *Numerical Prediction and Dynamical Meteorology* (2nd Ed.). Wiley and Sons, NY, ISBN 0-471-05971-4, pp. 477.

Klemp J.B., Wilhelmson R.B., 1978: Simulation of 3-dimensional convective storm dynamics. *Journal of Atmospheric Science*, 35:1070–1096.

Liu J., Chen J.M., Black T.A .and Novak, M.D., 1995: E-ε Modeling of turbulent air flow Downwind of a model forest edge. *Boundary-Layer Meteorology*, 77:21-44.

Patton E. G., Shaw R. H., Judd M. J. and Raupach M. R., 1998: Large-eddy simulation of windbreak flow. *Boundary-Layer Meteorology*, 87: 275-306.

Prueger J.H., Eichingerb W.E., Hippsc L.E, Hatfielda J.L., Cooperd D.I., 2008: Air-flow distortion and turbulence statistics near an animal facility. *Atmospheric Environment*, 42, 3301–3314.

Raynor, G.S., 1971: Wind and temperature structure in a coniferous forest and a contiguous field. *Forest Science*, 17:3:351-363.

Santiago J.L., Martin F., Cuerva A., Bezdenejnykh N., Sanz-Andres A., 2007: Experimental and numerical study of wind flow behind windbreaks. *Atmospheric Environment*, 41:6406–6420.

Shaw R.H., Patton E.G., 2003: Canopy element influences on resolved- and subgrid-scale energy within a large eddy simulation. *Agricultural Meteorology*, 115:5–17.

Shaw R.H., Schumann U., 1992: Large-eddy simulation of turbulent-flow above and within a forest. *Boundary-Layer Meteorology*, 61:47–64.

Walko R.L., Avissar R., 2008: The ocean-land-atmosphere model (OLAM). Part II: formulation and tests of the non-hydrostatic dynamic core. *Monthly Weather Review*, 136:4045–4062.

Yang B., Raupach M.R., Shaw R.H., Kyaw Tha Paw U., Morse A.P., 2006b: Large-eddy simulation of turbulent flow across a forest edge. Part I: flow statistics. *Boundary-Layer Meteorology*, 119:377–412. doi:10.1007/s10546-006-9083-3.